Materials Advances

ROYAL SOCIETY OF CHEMISTRY

PAPER

View Article Online
View Journal | View Issue

Cite this: *Mater. Adv.*, 2023, 4, 669

Evaluation of techniques used for visualisation of hydrogel morphology and determination of pore size distributions†

Imanda Jayawardena, [a] Petri Turunen,[bc] Bruna Cambraia Garms, [a] Alan Rowan,[c] Simon Corrie [d] and Lisbeth Grøndahl *[ac]

Received 28th September 2022,
Accepted 16th December 2022

DOI: 10.1039/d2ma00932c

rsc.li/materials-advances

This study evaluated three techniques, stimulated emission depletion (STED) microscopy, atomic force microscopy (AFM), and cryogenic scanning electron microscopy (Cryo-SEM), for visualising the morphology and obtaining pore size information of agarose hydrogels (0.38, 1.0, 1.5, 2.0% agarose content). The pore size distributions were obtained using a common manual approach which was validated for Cryo-SEM data using poly(lactic-*co*-glycolic acid) (PLGA) nanoparticles as an internal standard. There was good agreement in pore size distribution data for agarose hydrogels with an agarose content of 1.0% and higher when using these techniques. For the 1.0% gel sample imaged using STED and Cryo-SEM, no significant difference was observed between these two techniques yielding average pore sizes of 240 and 230 nm, respectively. The average pore size values obtained from AFM images for 1.5 and 2.0% gel samples were significantly smaller by 10–15% compared to values obtained from Cryo-SEM data as predicted due to the AFM tip artefact for concave features. Pros and cons of each technique are discussed in detail.

1. Introduction

Hydrogels consist of hydrophilic crosslinked polymer networks that are capable of adsorbing and retaining large amounts of water, in some cases >90%, which is significantly higher than that found in mammalian cells (*e.g.* 50–70%). The void space between polymer strands or polymer bundles is an important aspect in defining hydrogel properties. The size of this void space has been referred to as the pore size (referring to pore diameter) in some literature[1] while recently, Peppas and co-workers introduced the term mesh radius.[2] As the transport properties within gels are largely dominated by diffusion gradients, the pore size and pore size distribution of hydrogel materials are important design features for developing biomaterials with applications spanning diagnostic, therapeutic, drug delivery, and cell encapsulation.[3–9] Common to these applications is a need to control diffusive properties of small molecules and/or proteins through the hydrogel structure. In addition, the hydrogel morphology including the pore size distribution influences the mechanical properties such as compressive modulus and elongation. Therefore, in order to rationally design a hydrogel matrix for a specific application, the ability to accurately determine the pore size distribution is important, and few, if any, techniques have been properly validated to ensure the results are accurate.

Considering the experimental flow depicted in Fig. 1, it is evident that a number of aspects will have an impact on the hydrogel morphology and pore sizes that are reported. Many of these aspects are intentionally chosen in the design of a hydrogel with required properties such as the polymer chemistry, gelling conditions including the polymer concentration and the resulting degree of crosslinking (affected by *e.g.* concentration of crosslinker). Other factors are dictated by the technique used for characterisation, such as the requirement to label the polymer with a fluorescent dye, the degree of labelling and the ratio of labelled and unlabelled polymer in the hydrogel. The type of vessel (depth and width) may also affect the hydrogel structure, as may

[a] *School of Chemistry and Molecular Biosciences, University of Queensland, Brisbane, QLD 4072, Australia. E-mail: l.grondahl@uq.edu.au*
[b] *Microscopy Core Facility, Institute of Molecular Biology, Mainz, Germany*
[c] *Australian Institute for Bioengineering and Nanotechnology, University of Queensland, Brisbane, QLD 4072, Australia*
[d] *Department of Chemical Engineering, ARC Centre of Excellence in Convergent Bio-Nano Science and Technology, Monash University, Clayton, VIC 3800, Australia*

† Electronic supplementary information (ESI) available: Example of raw and deconvolved CLSM and STED images; examples of structures that can be visualised by Cryo-SEM or SEM after erroneous treatments; pore size determination using manual approach and intensity plots; determination of PLGA particle size in composite hydrogel; evaluation of a suitable binarization threshold for STED images; evaluation of bundle thickness; Cryo-SEM data for additional gel samples (1.5% replicate; 1.0% different agarose type and water *vs.* PBS); examples of agarose pore size data of studies reported in the literature. See DOI: **https://doi.org/10.1039/d2ma00932c**

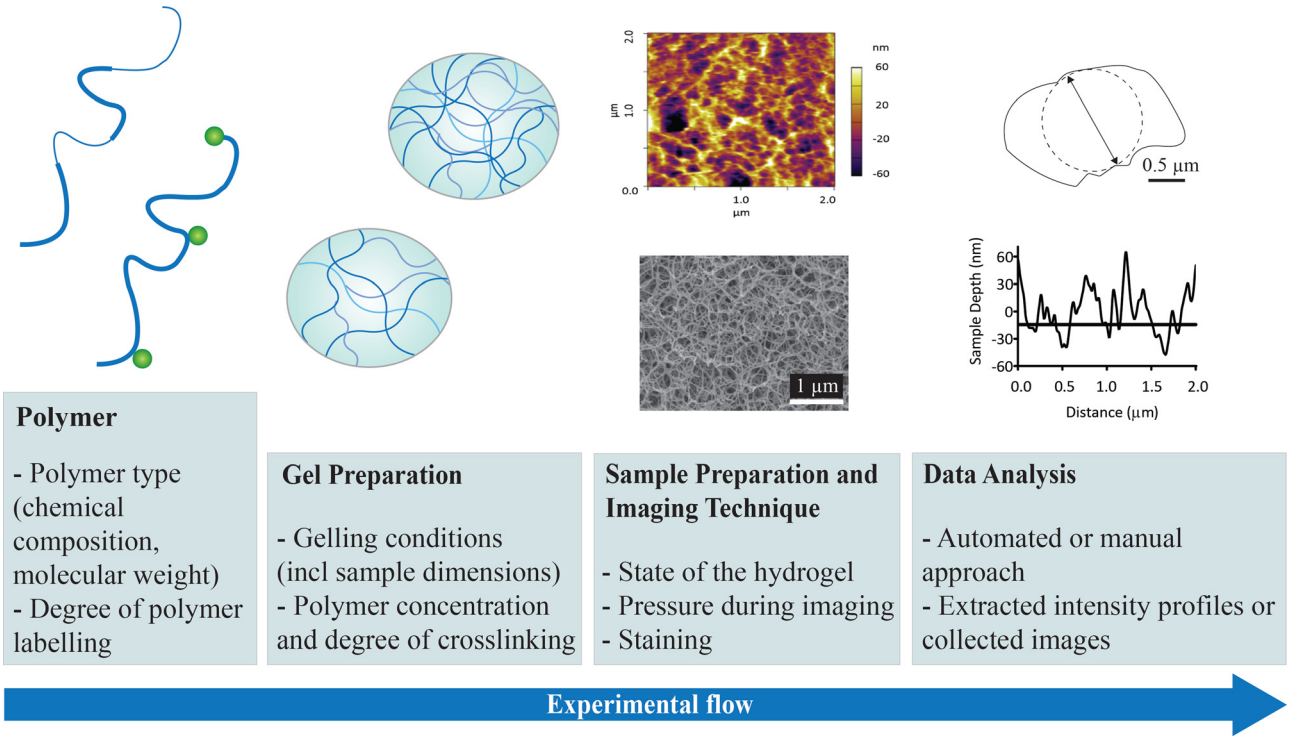

Fig. 1 Illustration of the experimental flow for obtaining pore size information of hydrogels and the factors that may affect the morphology and the pore size distribution that is reported.

the temperature and ionic strength used during gel preparation. Some imaging techniques require additional sample preparation including dehydration, freezing and fracturing, while other techniques allow imaging of the hydrogel structure in the native hydrated state at ambient conditions. The requirement for freezing water within a hydrogel sample or dehydrating a hydrogel poses challenges in characterisation of hydrogels. These processes have been widely recognised as common causes of structural damage to the hydrogel, resulting in imaging artefacts and overestimation of the hydrogel pore size by orders of magnitude. This includes formation of hexagonal ice crystals during freezing and creation of micron-sized pores during freeze drying.[1,3,6,8,10,11] The final aspect in Fig. 1 relates to data analysis which, depending on the data collected, may use a manual or an automated approach using either collected images directly or intensity profiles which are extracted from the data.

Characterisation techniques that have been applied for the determination of hydrogel pore size include both direct visualisation methods (*e.g.* electron microscopy) and indirect evaluation based on a bulk measurement (*e.g.* differential scanning calorimetry (DSC)). While direct imaging approaches allow direct measurement of many pores in a sample, thus building a model-free distribution, indirect approaches yield pore size data as the output of various models.[12,13] An important distinction between the information gained is that when applying direct visualisation methods a pore size distribution is obtained, while when applying indirect evaluations only a mean or lower limit value is calculated.[12–14] As hydrogels do not contain uniform pores, with respect to size or shape, a pore size distribution is much more informative. Cryogenic scanning electron microscopy (Cryo-SEM) is a common approach, however, issues involving the introduction of artefacts during either sample preparation or the imaging process (*e.g.* under vacuum), require innovative approaches to ensure that the native structure is captured. Our work on imaging alginate hydrogels demonstrated that the use of high-pressure freezing avoids creation of known freezing artefacts,[1] and a subsequent study highlighted the correlation between such artefacts and hydrogel properties (*e.g.* modulus and water content).[11] Fluorescence microscopy approaches provide the opportunity to image gels under native conditions, yet require the introduction of a fluorescent label[15] which may introduce artefacts. Furthermore, the *x*–*y* resolution of confocal laser scanning microscopy (CLSM) is 200 nm at best which is not always within the pore size range of hydrogels, hence super-resolution approaches including stimulated emission depletion (STED) microscopy[16–20] may be required to reduce resolution-based errors. The use of atomic force microscopy (AFM) for the measurement of hydrogel pore size distributions is less commonly applied, even though the approach allows for imaging of the hydrogel in its native state without the need for labelling and without resolution issues. While AFM is optimised for studies of stiff materials, the cantilever of the AFM can be adjusted, enabling its use with hydrogels which are inherently soft.[10]

Data analysis is an important component in the evaluation of the pore size distribution of hydrogels and can significantly affect the pore sizes that are reported. A common issue with most approaches is how to determine the dimensions of a 3D pore from

a 2D image. Studies have indicated that pore sizes determined from the same images using either a 2D or a 3D approach differ by less than a few percent validating the use of the simpler 2D methods.[21,22] There are different approaches that have been used to extract pore size information from a data set. The first aspect to consider is if a 2D image or an intensity profile (Fig. 1) will be used for the analysis, the latter being easily available from the data generated by *e.g.* AFM and STED. When the 2D image is used for analysis, it can be analysed by either a manual[1] or an automated[23] approach. Inherent in all data analysis, is the choice of a threshold that defines where the pore wall ends and the pore void starts.

The current work uses physical hydrogels made from agarose and complements our previous study investigating calcium cross-linked alginate hydrogels.[1] It represents a gel of low modulus and high water content that is prone to the introduction of freezing artefacts during sample preparation for Cryo-SEM.[11] Agarose has a long history of applications in biomedical research particularly for DNA gel electrophoresis and continues to be applied as a model hydrogel system.[24–26] It consists of an uncharged linear polysaccharide extracted from red algae, made from monomer units of D-galactose and 3,6-anhydro-L-galactose.[27] Gels form at temperatures around 35 °C and at concentrations as low as 0.1%,[27] with commercial reagents selected for "high" and "low" gelling temperatures. The gelling process is physical and is brought about by hydrogen bonding between the agarose molecules leading to the formation of networks.[28] Agarose hydrogels are best described as biphasic gels, one phase being solvent-rich and the other a polymer-rich phase.[29,30] This means that the walls of agarose hydrogels are not solid and as such the bundle thickness cannot be used to calculate pore size in a meaningful way, however, it is a useful metric that we can compare to our images obtained by the different techniques. Previous studies using Cryo-TEM, Cryo-SEM, SAXS/SANS or AFM, have reported the bundle thickness for agarose gels to be 5–20 nm.[31–33]

There is a need to evaluate the techniques used for visualising hydrogel morphology and their ability to provide correct information about the native structure of hydrogels. Considering the articles citing our previous article[1] on the use of high-pressure freezing of alginate hydrogels prior to Cryo-SEM evaluation, the challenge of capturing the native hydrogel structure is well recognised, yet only few studies have adopted this method.[34–36] This lack of access to high-pressure freezing equipment has motivated us to compare established as well as emerging direct imaging techniques in order to provide additional guidance on hydrogel imaging. This manuscript thus investigates, in-depth, three different techniques used for capturing images of agarose hydrogels, namely Cryo-SEM, STED microscopy and AFM. Manual image analysis is used as the common approach to extract pore size information across all data sets.

2. Materials and methods

2.1 Materials

Agarose for immunoelectrophoresis, low EEO (gelling temperature 34–38 °C, Product Number: A4679, Catalogue Number: US024566, Sigma-Aldrich), PLGA-E1 (poly(lactic-*co*-glycolic acid), Resomer® RG 502, ester terminated, M_W = 7–17 kg mol^{-1}, T_g = 42–46 °C, Sigma-Aldrich), poly(vinyl alcohol) (PVA, M_W = 25 kg mol^{-1}, 88% hydrolysed, Polysciences Inc.), 10 × Phosphate Buffered Saline (PBS, Bio-Whittaker), 5-(4,6-dichlorotriazinyl) aminofluorescein (5-DTAF) (Thermo Fisher Scientific), absolute ethanol (Merck), Na_2SO_4 (99% purity, Chem Supply), NaOH (98% purity, Chem Supply), hexadecene (Merck), dichloromethane (DCM, anhydrous, ≥98%, Merck) and deionized (DI) water were employed in the experiments. Minor alterations were made to the procedure for labelling agarose with fluorescent 5-DTAF.[37] Specifically, the labelled agarose polymer was washed thoroughly with DI water in addition to an ethanol wash, to ensure the removal of the salts precipitated during the labelling process, and the efficiency of the process was verified using FTIR spectroscopy. According to the published work, this process results in labelling every 200th monomer.[37]

2.2 Material fabrication

In the current study, in order to achieve homogeneous hydrogels, a homogeneous agarose solution was prepared by heating on a water bath at 110 °C for 30 minutes with continuous magnetic stirring, rather than by the standard microwave method. Agarose hydrogels form upon cooling, and the final gel structure and pore size distribution are affected by the cooling rate.[38,39] In the current study, the gel was formed with rapid cooling over 30 min from 72 to 30 °C, followed by a very slow cooling phase until the hydrogel reached 22 °C (the cooling curve was previously published[9]). Separate agarose gels prepared from agarose solutions of various concentrations (0.38–2.0% w/v) are referred to as agarose gels of the respective concentration. For example, for a '1.0% agarose gel', 50 mg of agarose powder was dissolved in 5 mL of 1 × PBS. Solutions of varying concentration were all made using a volume of 5 mL. The solutions were cast in suitable moulds depending on the imaging technique to produce translucent gels of varied thickness. For Cryo-SEM (gel thickness: 7.75 mm), flat bottom 48 well microplates, well diameter: 1.1 mm (Nunclon Delta Surface, Thermo Fisher Scientific) were used. For AFM (gel thickness: 1.15 mm), 50 × 9 mm style Petri dishes, diameter: 50 mm (BD Falcon) were used. For STED/CLSM (gel thickness: 2.29 mm), 35 mm glass-bottom microwell dishes, diameter: 35 mm (MatTek Corporation) were used.

PLGA nanoparticles were prepared by an emulsion solvent evaporation technique as previously published.[40] Briefly, 10 mg PLGA was dissolved in 0.5 mL DCM (20 mg mL^{-1}). This solution was added dropwise to a surfactant solution containing 1.0% w/v PVA (20 mg) in 2 mL of DI water whilst stirring. The emulsion was sonicated in an ice bath using a Branson Digital Sonifier 450 with a 1/8″ tapered microtip operated at 20% amplitude (179 μm) for 2 minutes. The resulting particle suspension was added dropwise into 40 mL of DI water and magnetically stirred for 3 hours to allow evaporation of the organic solvent. The emulsion was centrifuged at rcf = 76 500 × *g* for 1 hour maintained at 17 °C on a Beckman Coulter Avanti

HP-20 with a JA25.50 fixed angle rotor and washed twice. The washed particle pellet was resuspended in 1 mL of DI water.

The agarose gel containing nanoparticles and a control gel were prepared in DI water at an agarose concentration of 0.38%. To prepare the composite gel, a nanoparticle suspension was added to the agarose solution such that the final PLGA nanoparticle mass in 2 mL was 4.5 mg. Solutions of agarose or agarose containing the nanoparticle suspension (2 mL) were cast in 35 × 10 mm Petri dishes, diameter: 35 mm (gel thickness: 3.0 mm).

2.3 Sample preparation and imaging

2.3.1 STED. STED (and simultaneous CLSM) imaging of agarose hydrogels were conducted with the use of the fluorescent dye 5-DTAF ($\lambda_{ex/em}$ = 492/516 nm). Gels were prepared from labelled agarose only. The gels were imaged in their hydrated state in air at ambient humidity and temperature. Imaging was performed using Leica TCS SP8 STED 3× confocal microscope system, equipped with white light laser (WLL), STED laser of 592 nm and Leica hybrid detectors for single molecule detection (HyD SMD). Images were captured using 100 × 1.4NA oil immersion objective. The combination of imaging with high NA objective and using only labelled polymer was found to allow for much greater detail of the hydrogel network, than what was previously reported using a 1 : 4 ratio blend (labelled to unlabelled agarose) and imaging using a 60 × 1.2NA water immersion objective.[37] In more detail, imaging was performed in the resonant scanner mode with 32-line averaging. The 488 nm line from WLL was used for excitation and fluorescence emission was collected from 495–585 nm band. For each region, images was first captured in confocal mode, followed by STED. For STED imaging, 60% of the STED laser power was used. Three regions from each hydrogel sample were imaged, with the 1032 × 1032 pixel format (pixel size of 29 nm) for each region, representing an area of 30 μm × 30 μm as the *z*-stack of three slices with an interval of 219 nm. The focus plane (center slice) was set to 5 μm above the coverslip. This was found to be a sufficient distance from the coverslip to avoid any surface proximity effect on the hydrogel and not too far in solution such that any image quality degradation due to refractive index mismatch of the oil objective could be avoided. The *z*-stack thus acquired provided 3D information for the subsequent deconvolution step. A deconvolution approach was successfully applied to increase the signal-to-noise ratio and to improve the resolution of raw agarose hydrogel images as previously described.[41] An example is included in the ESI† (Fig. S1). Briefly, the images were deconvolved using the Huygens Professional (Scientific Volume Imaging, the Netherlands) software in wizard mode (CMLE algorithm, max. iterations 80, quality criteria 0.05, SNR 10 for confocal and SNR 7 for STED). A single deconvoluted 2D slice for each region was used for subsequent analysis.

2.3.2 AFM. The contact mode of AFM was used to image the surface of agarose gels immersed in DI water at ambient temperature. Contact resonance mode for imaging softer materials is preferred as this will ensure constant contact between the tip and the sample.[42,43] The presence of water prevents the evaporation of water from the gel surface and helps eliminate the capillary forces between the cantilever tip and the gel preventing dehydration of the gel.[44] AFM imaging was achieved using an MFP-3D AFM (Asylum Research, USA) mounted on an anti-vibrational table (Herzan, USA) and operated within an acoustic isolation enclosure (TMC, USA). Silicon nitride cantilevers (Budget Sensors, Bulgaria) with a triangular tip, a nominal spring constant of 0.06 N m^{-1} and a resonant frequency of 10 kHz were used. The force constant is an important parameter in AFM imaging; where softer cantilevers exert less pressure on the sample compared to a stiff cantilever, making them more suitable for imaging softer materials such as hydrogels.[42] The forces exerted on to the gel by the cantilever tip were minimised in order to avoid any potential damage to the surface of the gel. It should be noted that due to the manner in which the AFM tip scans across a porous surface, the reported artefact of pore narrowing results in more narrow and shallow troughs compared to the actual pore.[42,45] Three regions of 2 × 2 μm were imaged for every sample.

2.3.3 Cryo-SEM. High-pressure freezing (HPF) and Cryo-SEM imaging were performed based on the procedure previously published.[1] A sample with the dimensions 0.1 cm × 0.1 cm × 0.026 cm (width × length × height) was cut from the gel and transferred to a brass HPF sample holder. The space between the sample and the sample carrier was filled with hexadecane to ensure no voids remained during freezing. The sample container was clamped to an arm assembly and transferred to the primed high-pressure freezer (Baltec HPM010), where the specimen was frozen under a stream of liquid nitrogen at a pressure greater than 2100 bar. Subsequently, the arm assembly was removed from the freezer and the sample carrier was immediately plunged into a liquid nitrogen filled carrier to prevent any warming up of the sample. The high-pressure frozen samples were stored under liquid nitrogen until imaging. During Cryo-SEM imaging, the top of the sample carrier was removed, while gently clamped to a brass ALT 118 Gatan sample holder under liquid nitrogen, to expose the dome of the frozen sample within the brass carrier. While still under liquid nitrogen the sample was mounted on a Gatan Alto sample holder (ALT 136) and transferred under vacuum to the Cryo-SEM preparation chamber which was maintained at less than 100 K. The exposed dome was fractured within the chamber, using a Gatan precision cold rotary knife ALT 335, to provide a clean, uncontaminated section of the internal structure of the gel. This fracturing is a random process through the horizontal plane of the gel and a transverse section is revealed. A JEOL JSM-7100F field emission scanning electron microscope coupled to a Gatan Alto 2500 cryotransfer chamber was used to image the samples, at a low accelerating voltage (*e.g.* 2 kV) and a spot size of 3. Based on the optimised procedures, sample sublimation was carried out for 60 minutes at −105 °C within the SEM chamber and subsequently the samples were sputter coated twice with Pt for 120 s at 10 mA. Three or four regions at 30 000 times magnification were imaged for every sample. This magnification was chosen as a

practical compromise between image resolution, number of pores per image, and minimising sample charging effects (no additional information could be obtained from an image at 60 000 times magnification). Each image covered approximately 4×5 μm.

Included in the current study are SEM images obtained for samples for which we deliberately introduced various artefacts from drying or freezing of hydrogel samples in order to have these as reference images and these are included in the ESI† (Fig. S2). Specifically, when using critical point drying, we have observed that this process significantly contracts the hydrogel specimen in an irregular manner. We therefore recommend, that the pore size distribution that can be obtained from the resulting images is not re-scaled to the dimensional changes of the overall hydrogel.

2.4 Pore size determination

In the current study, the term 'pore size' refers to the diameter of a sphere that fits within a specific pore. The distribution of pore sizes measured within a region of interest in a given hydrogel sample is referred to as a 'pore size distribution'. The 'homogeneity' of the pore size distribution of a gel sample refers to a statistically non-significant distribution of pore sizes throughout a gel sample of a given concentration (further detail provided in Section 2.6). The manual approach to determination of the pore size distribution used ImageJ software as previously described.[1] Illustration of this approach can be found in the ESI† where it is applied to a Cryo-SEM image (Fig. S3, ESI†). The current study involved two researchers who cross-referenced their interpretation of the images and how to place the circle.

For images obtained by Cryo-SEM, only pores belonging to the topmost porous network were considered. This distinction is important as the Cryo-SEM images reveal underlying layers of porous networks of the gel where individual pores are more difficult to distinguish and may be obscured by the topmost network. This issue does not present itself with respect to evaluating the STED and AFM images as they do not display underlying porous networks. For these techniques, a threshold that defines where the pore wall ends and the pore void starts needs to be chosen. For AFM images, we interpret the yellow to orange regions (Fig. S4, ESI†) as the pore walls and regions appearing black or dark purple (z-dimensions of -60 to -30 nm) as the pores. Deconvoluted STED images were binarised using thresholds ranging from 100% to 10%, decreasing the percentage by 10% in each step. Similar to the approach used by Vandaele *et al.*,[23] we assessed by visual inspection the quality of different thresholds and found that the 60% threshold had the highest degree of similarity (details included in ESI,† Fig. S5). For all image types, all pores within a selected region were measured to minimise bias.

2.5 Nanoparticle size determination

The particle size of the nanoparticles in the suspension was evaluated prior to gel preparation. This was done using dynamic light scattering (DLS) with a Malvern Zeta Sizer (Nano-ZS or Ultra or 3000 HSA) at 25 °C. The refractive index of the dispersing medium was set at 1.33 (water at 25 °C) and PLGA at 1.45. The sample was analysed at 25 °C with 3 repeat measurements.

The particle size of the nanoparticles in the gel was evaluated using a manual approach for SEM images captured at magnifications of 30 000×. A circle drawn using ImageJ software was placed on each nanoparticle, which displayed well-defined edges to determine the area which allowed the calculation of the diameter of the nanoparticle (details included in Fig. S6 in the ESI†). The scale bar of the images was used to calibrate the measured diameter to nanometres. All suitable nanoparticles of three images were counted.

2.6 Statistical analysis

Graphs were prepared in Prism 7 (GraphPad Prism 7.0). The manual approach was used to evaluate the pore size distribution from the images. Between 50 and 100 pores were measured and compared for each region. To evaluate the homogeneity of the pore size distribution of a gel, the pore size distributions obtained for various regions of a particular gel sample were evaluated *via* a statistical approach. Kruskal–Wallis analysis was performed to compare pore size distributions between regions of the same sample (n = 3 for AFM/STED/Cryo-SEM (with nanoparticles); n = 4 for Cryo-SEM), or to compare the methods. Error bars are expressed as standard deviation of the mean. For the DLS data where three repeat measurements were done on the particle suspension, the standard deviation and the mean represent the data from one such measurement and all three measurements gave similar values. The p-values obtained from all tests were interpreted by considering $p > 0.05$ to be a significant difference and $p \leq 0.05$ not to be a significant difference among the data sets being compared.

3. Results

3.1 Evaluating the morphology of agarose hydrogels using STED

Similar to CLSM, STED microscopy provides images of hydrated hydrogels in air at ambient conditions (temperature and humidity). The technique requires fluorescent labelling of the agarose polymer prior to gel formation and thus the agarose hydrogel substrates were prepared using 5-DTAF-labelled agarose. STED images were found to reveal more structural detail compared to the CLSM images, due to the enhanced resolution of the STED technique. This is clearly evident in Fig. 2A–D which displays CLSM and STED images of the exact same region of each hydrogel. Two hydrogels with different concentrations were imaged using this method, 1.0 and 0.38% agarose. These gels were found to have pore sizes above 143 nm (identified using Cryo-SEM, Section 3.3), which is more than three times larger than the pixel size in the STED imaging. Thus, the chosen conditions should provide sufficient sampling that potentially allow for accurate pore size determination from the STED images. The enhanced resolution provided by

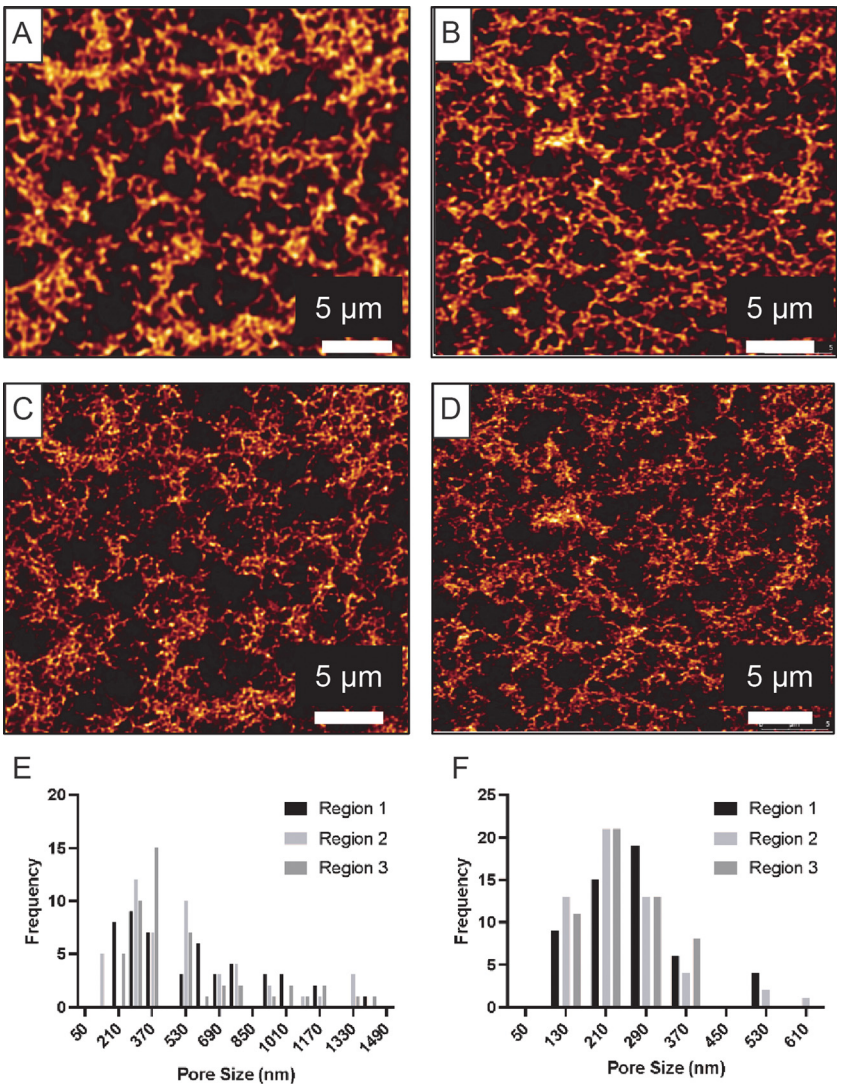

Fig. 2 Simultaneously captured deconvoluted STED and CLSM images. (A and B) CLSM images of gels prepared using different agarose percentages. (C and D) STED images of the same gels. (E and F) Display the pore size distributions for the STED images. (A, C and E) 0.38% agarose gel; (B, D and F) 1.0% agarose gel.

STED microscopy allows for detection of small pores that would be un-noticeable in regular CLSM images and evaluation of the pore size distribution was therefore restricted to the STED data. Some images captured of the 0.38% gel revealed what appeared to be channels throughout the structure indicating that the structure may have partly collapsed due to dehydration.

Statistical analysis of the pore size distributions obtained from STED (Fig. 2E and F) allow us to compare the degree of homogeneity between different regions of a given gel. The results displayed in Table 1 suggest that the gels were relatively homogenous for both agarose concentrations of 0.38% and 1.0%, based on a Kruskal-Wallis test. Wilcoxon tests of 1.0% and 0.38% gel pore sizes indicated a significant difference between the two concentrations (p-value < 0.0001), in agreement with their appearance in Fig. 2. It can be seen that the pore size distributions are skewed towards higher values consistent with a lognormal distribution, hence it is informative to also report the median values which are 400 nm for the 0.38% gel and 200 nm for the 1.0% gel.

3.2 Evaluating the morphology of agarose hydrogels using AFM

For AFM, no sample preparation is required and this technique permits the surface of the hydrogels to be imaged at ambient conditions where the gel is immersed in a suitable solution. AFM has previously been used to image agarose gels where pore size evaluation has mostly been done using a line plot.[31,33,44,46] A comparison to the line plot is included in Fig. S4 and S7 (ESI†). Two agarose gels were imaged using this technique, 1.5 and 2.0%, based on the requirement for a high polymer content. AFM images for agarose gels were captured based on reported imaging procedures combined with instrument-specific optimisations (Fig. 3A and B). An estimation of the bundle thickness was done for the 1.5% gel was found to be 35 nm ($n = 5$). The method used is described in the ESI† and images displayed in Fig. S8.

Table 1 Average pore size data[a] and evaluation of the homogeneity of the pore size distribution of the gels using the manual pore size determination approach

	STED[b]		AFM[c]		Cryo-SEM[d]	
Agarose (%)	Pore size (nm)	KW test *p*-value[e]	Pore size (nm)	KW test *p*-value	Pore size (nm)	KW test *p*-value
0.38	550 ± 330	0.86	—	—	380 ± 60	<0.0001
1.0	240 ± 110	0.21	—	—	230 ± 30	<0.0001
1.5[f]	—	—	170 ± 40	0.07	190 ± 25	0.35
					200 ± 30	0.22
2.0	—	—	130 ± 25	<0.0001	150 ± 50	0.23

[a] For the average pore size, errors are the standard deviations of the data combined from 3 or 4 regions of each gel. [b] $n > 100$. [c] $n > 150$. [d] $n > 300$. [e] Kruskal–Wallis (KW) test *p*-values indicate agreement between regions of a single gel, it was evaluated if the number of pores or number of regions analysed affected the statistical analysis but no effect was found. [f] Two replicate gels of 1.5% were analysed using Cryo-SEM.

Pore size data is displayed in Fig. 3C and D where the resulting histograms for three regions of each gel are included. The average pore size is included in Table 1. Analysis of different regions of one gel sample revealed that the 1.5% agarose gels were relatively homogenous, whereas there was a significant difference in the pore size distributions for the 2.0% gels across different regions (Table 1). This analysis was consistent even after removal of four extremely large pores from the data describing the 2.0% agarose gel, which were reasoned to be artefacts. On the basis of pooled pore size distribution for the 1.5% gel *versus* the 2% gel, Mann–Whitney tests indicated a significant difference in the pore size for the two types of gels (*p*-value < 0.0001).

3.3 Evaluating the morphology of agarose hydrogels using Cryo-SEM

Evaluation of hydrogel morphology using Cryo-SEM requires the use of high-pressure freezing and allows imaging of a cross-section of the gel. Agarose gels prepared from agarose solutions with concentrations of 0.38, 1.0, 1.5% and 2.0% could all be imaged and as such, data obtained from this technique can be compared to STED and AFM. The images and pore size distributions obtained are shown in Fig. 4. A bundle thickness of 36 nm ($n = 5$) was obtained for the 1.0% gel (Fig. S8, ESI†). The average pore size values obtained are given in Table 1. Furthermore, Table 1 also includes values for a replicate sample of a 1.5% agarose gel. The images and pore size distribution plots for three regions of this true repeat sample are included in Fig. S9 (ESI†).

The homogeneity of the pore size distribution of the gels as a function of agarose concentration was evaluated using a Kruskal–Wallis analysis. For both the 1.5% and the 2% agarose gels it was found that there were no significant differences in pore size distributions collected from different regions (Table 1). However, in the case of the lower agarose concentrations (0.38 and 1.0%), there were significant differences

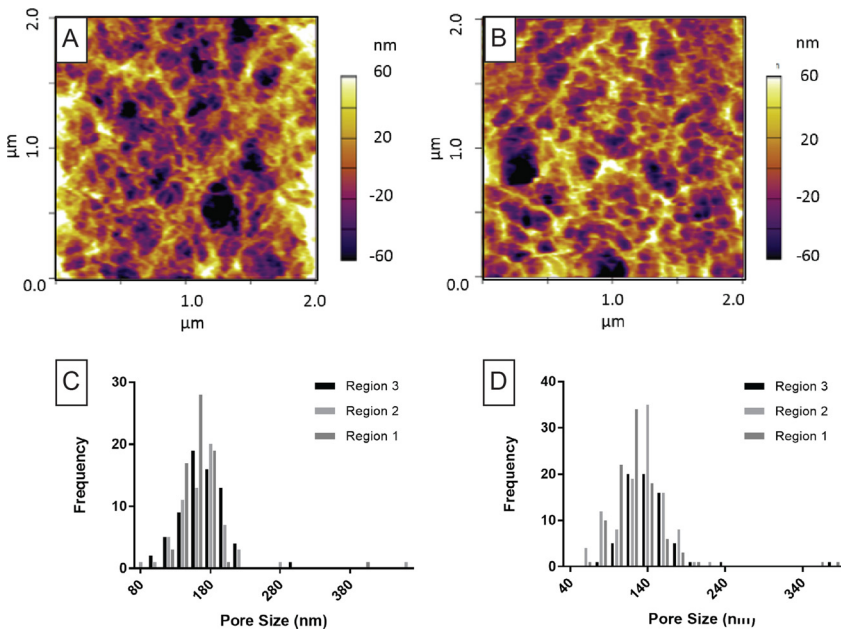

Fig. 3 (A and B) AFM images of gels prepared using different agarose percentages (horizontal and vertical scale bars: 2 µm, the depth scale is indicated on the right-hand side of each image as a coloured bar). (C and D) Display the pore size distributions determined using the manual approach. (A and C) 1.5% agarose gel (B and D) 2% agarose gel.

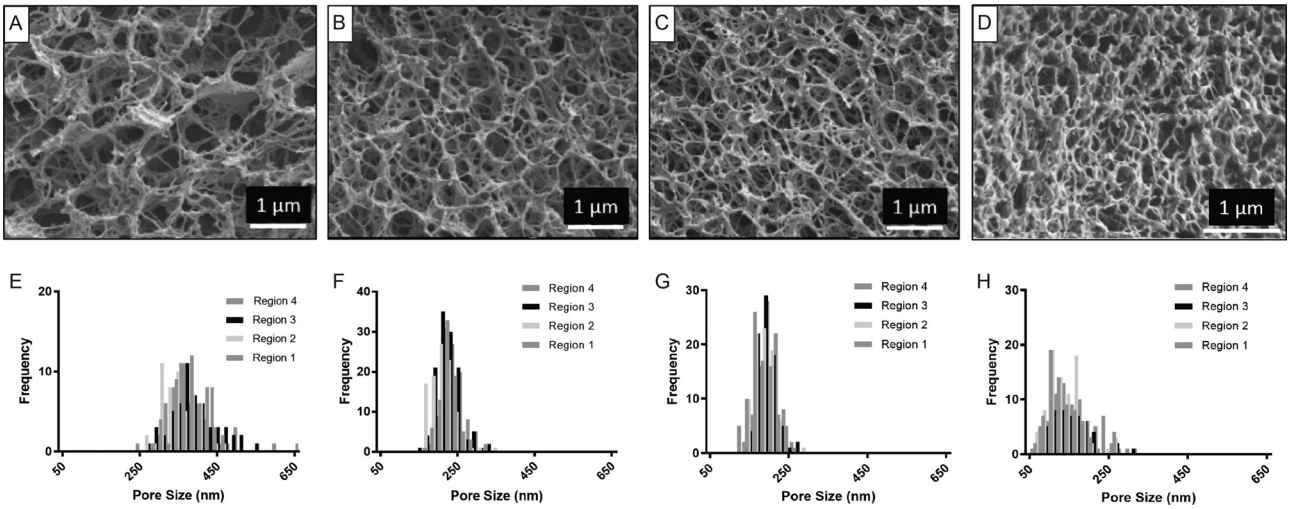

Fig. 4 (A–D) Cryo-SEM images at 30 000× magnification (scale bar: 1 μm). (E–H) Display the respective pore size distributions determined using the manual approach. (A and E) 0.38% agarose gel; (B and F) 1.0% agarose gel; (C and G) 1.5% agarose gel; (D and H) 2.0% agarose gel.

between regions, suggesting that these samples were less homogenous. Kruskal–Wallis tests indicated significant differences of the pore size distributions for all five gels evaluated including those prepared using different agarose concentrations as well as the replicate samples (p-value < 0.0001). Therefore, despite the average pore size values for the replicate samples differing by only 5%, the pore size distribution is significantly different. This highlights the combined errors associated with sample preparation, gel preparation by HPF and coating, and manual pore size determination.

3.4 Evaluation of pore size distribution by Cryo-SEM in hydrogels containing nanoparticles

To evaluate the suitability of using the manual approach for determination of the pore size distribution, we created a 0.38% agarose gel (from water) containing PLGA nanoparticles with a size distribution pre-determined by DLS (Fig. 5A). These nanoparticles made from PLGA were used as an internal standard of size as this particle is not subjected to swelling in water and as such would be minimally impacted by the freezing preparation.[47,48] We found excellent agreement with DLS when we measured the particle size distribution using the manual approach applied to the Cryo-SEM images (Fig. 5B). Our previous work evaluating this type of PLGA nanoparticles likewise confirmed that there was no difference in the size obtained from dried particles imaged *via* SEM and a particle suspension evaluated using DLS of the same particle batch.[40] Collectively, this confirms that the particle size was not affected by the high-pressure freezing process, nor by the presence of the hydrogel.

The hydrogel morphology can be observed in Fig. 5C (control hydrogel) and Fig. 5D (hydrogel with particles) together with pore size distribution evaluated using the manual approach shown in Fig. 5E (control hydrogel) and Fig. 5F (hydrogel with particles). The Kruskal–Wallis test showed that there was no significant difference among three regions of agarose hydrogels containing nanoparticles (p-value > 0.05). Similarly, the control sample was homogeneous between two regions of the samples when analysed by the Mann-Whitney test (p-value > 0.05). The presence of the PLGA nanoparticles did not have a significant effect on the pore size distribution. The control hydrogel had an average pore size of 135 ± 65 nm while the hydrogel with nanoparticles had an average pore size of 140 ± 55 nm which was not significantly different (p-value > 0.05). In addition, it was observed that the size range of the nanoparticles fell within the size range of the hydrogel pores making them a suitable internal reference.

4. Discussion

The current study aimed to evaluate the effect of the measurement technique (*e.g.* Cryo-SEM, AFM and STED) on the hydrogel morphology and pore size distribution. The pore diameters of the agarose gels were defined as the smallest diameter of the void space enclosed within the pore walls. This way of defining the pore size agrees with the mesh radius recently introduced by Peppas and co-workers.[2] This definition of the pore size is useful when the value is used to correlate diffusion of solid nanoscale objects through the hydrogel. It is, however, different to the Feret diameter[49] and depending on the shape of the pore, the pore size may be underestimated relative to that of the Feret diameter. To avoid introducing additional variables in the study, a common approach to extracting the pore size from the images generated from the different techniques was required. A manual approach as proposed in our previous work[1] was found to allow pore size information to be extracted from all image types in the current study.

The level of morphological detail for the hydrogels captured by different techniques is distinctly different. The enhanced depth sensitivity of SEM yielding almost 3D information permits a clear visualisation of the pore walls and pore void compared to AFM or STED which are less depth-sensitive

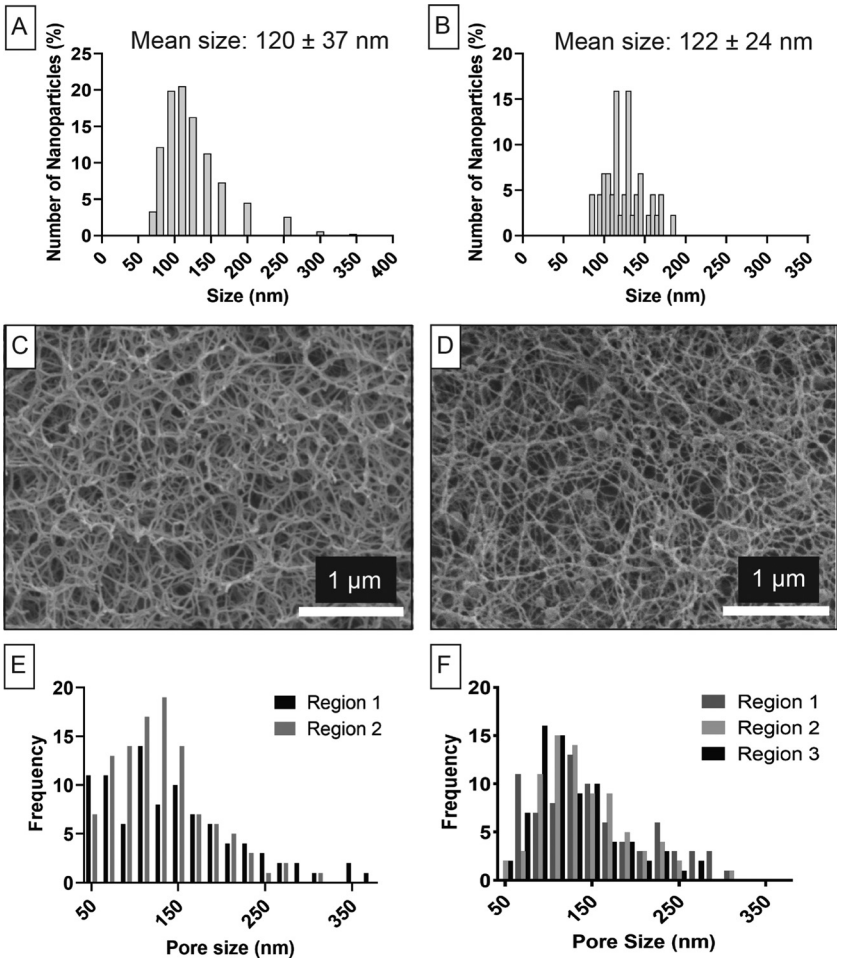

Fig. 5 (A) Hydrodynamic size distribution of nanoparticles determined by DLS prior to hydrogel formation. (B) Size distribution determined from the manual approach for nanoparticles in the gel where n = 42. (C) Cryo-SEM image of control sample of 0.38% agarose hydrogel at 30 000 × magnification (scale bar: 1 μm). (D) 0.38% agarose hydrogel containing PLGA nanoparticles at 30 000 × magnification (scale bar: 1 μm). (E) Pore size distribution determined using the manual approach of the control sample. (F) Pore size distribution determined using the manual approach of the hydrogel containing PLGA nanoparticles.

techniques where the pore walls and boundaries are less well defined. STED images (Fig. 2) display a network structure with 'walls' of approximately 1–2 μm surrounding large pores. The 'walls' appear not solid but rather porous with much smaller pores. The AFM images (Fig. 3) look somewhat similar to the STED images although the scale is very different with the 'walls' being much thinner and less than 200 nm and they appear less porous. SEM captures images that reveal a very detailed porous network structure (Fig. 4) with no evidence of similar 'wall' structures. The bundle thickness obtained from the AFM and SEM images gave similar average values of 35–36 nm for both techniques while the pixel size of the STED images did not allow for this analysis. It has been recognised that the bundle thickness depends on agarose concentration[31] and as such, our measurement is in general agreement with those previously found (5–20 nm.[31–33]). This is a key measurement which allows validation of the images captured by SEM and AFM in the current study.

The homogeneity of the pore size distribution of the gels was evaluated (Table 1). An increase in homogeneity with increasing agarose concentration has previously been observed for agarose gels.[44,50] This trend was supported in this study by the Cryo-SEM data for which we had four different gel concentrations. In addition, it was found that the 0.38% gels with nanoparticles prepared in water and imaged using Cryo-SEM were homogeneous. Since the pore size of this gel is significantly smaller (140 ± 55 nm) compared to the one prepared from a PBS solution (380 ± 60 nm) the level of homogeneity appears to be related to the pore size, as per the expected and confirmed trend. For the data obtained from AFM and STED data, it is more difficult to evaluate this trend as each technique was applied only to two gel samples.

The pore size distributions for the gels prepared from PBS solutions were given in Table 1 and the distribution plots in Fig. 2–4. Due to the increased resolution, super-resolution imaging techniques such as STED microscopy[16–18,51,52] provides more structural detail of the hydrogel network. This allows for detection of small pores that would be un-noticeable in regular CSLM images, leading to more accurate representation of pore size distribution when using STED. For data

obtained by each technique of this study (STED, AFM, Cryo-SEM), there were statistical differences between the pore size distributions obtained from images captured of different gel concentrations (p-value $\leq$ 0.001). All data follow an inverse relationship between the agarose concentration and the pore size, consistent with expectations.[33,37,44,46,50,53,54]

In the current study, PLGA nanoparticles served as an internal reference in addition to the scale bar. Similar use of particles as internal magnification standards has been reported for decades in electron microscopy.[55,56] Monodispersed polystyrene spheres can be fabricated with a well-defined diameter that range from 80 nm to 90 μm and are extensively used for this purpose.[57–60] In the current study, the size of the PLGA nanoparticles was 120 nm which falls within the range of pore sizes observed in the hydrogels making these particles a suitable internal standard. The use of this internal standard further confirmed the suitability of using the manual approach for determining pore size distributions from Cryo-SEM images. Incorporation of PLGA nanoparticles in 0.38% agarose gels in the current study found no change in hydrogel structure or pore size distribution. However, it is possible, that if higher nanoparticle loadings are used or if the nanoparticles have strong intermolecular interactions with the hydrogel matrix, that alteration to the hydrogel network could occur and it is recommended that this aspect is evaluated.

The main aim of the current study was to compare the pore size distribution obtained by different techniques. For the 0.38% gel, a significantly larger average pore size was obtained from images captured by STED compared to Cryo-SEM (p-value $\leq$ 0.001), where the relative difference in size was 45%. In contrast, for the 1.0% gel sample, there was no significant difference observed between these two techniques (p-value 0.94, data pooled across replicates). The average pore size values obtained using AFM and Cryo-SEM for 1.5 and 2.0% gels were significantly different (p-value $\leq$ 0.001), with a 10–15% difference between the two techniques, where the pore size distributions were more narrow and the average pore sizes smaller when using AFM. This smaller size obtained from AFM images can be justified considering the expected underestimation of the pore size due to the AFM tip artefact for concave features.[61] An important observation of this study is that despite the differences in the morphological details of the hydrogels in the images captured by STED, AFM and Cryo-SEM, for gels of 1.0% agarose or higher, the pore size distributions are in close agreement with each other (less than 15% different). Based on the accepted trend that lower agarose concentrations lead to less regular porous networks, there is expected to be more experimental variation between techniques and even replicates for $<$1.0% agarose gels, and perhaps also a larger effect related to the sample preparation method such as the casting substrate, gel dimension and imaging environment.

There are studies in the literature reporting the pore size of agarose gels employing CLSM[37] and AFM[33] as well as indirect methods[50,53,62–64] where freezing artefacts are not a contributing factor. Yet, these studies report pore diameters for agarose gels prepared from a 1.0% agarose concentration in the range from 150 nm to 1 μm (refer to ESI,† Table S1). While it is acknowledged[37,44,46,53,65] that many parameters including the type of agarose, the concentration of agarose and the ionic strength of the casting solution affect the pore size, we have determined that these parameters account for a variation of pore diameter from 130 to 380 nm based on HPF and Cryo-SEM imaging (data included in main manuscript Table 1 and Section 3.4 and in ESI,† Fig. S10). This is a significantly smaller range than that previously reported. The parameter to cause the most pronounced effect based on our data is the ionic strength of the casting solution. Thus, the pore size of the 0.38% agarose gel prepared from a PBS solution was 380 $\pm$ 60 nm (Section 3.3) while the gel prepared from water was 130 $\pm$ 60 nm (Section 3.4).

The techniques evaluated in the current study each have some shortcomings, and it is therefore critical to report, and where possible investigate, parameters that may affect the pore size distribution that is obtained. This includes the hydrogel preparation (*e.g.* using labelled agarose), sample preparation (*e.g.* HPF, casting substrate), imaging conditions (*e.g.* under vacuum and at low temperature or in the native state in air), imaging region (surface or internal structure) which are all aspects that can cause introduction of systematic errors. As a summary, Table 2 outlines advantages and disadvantages of the techniques based on investigations of the current study and previous work.

In general, imaging of a hydrogel in its native hydrated state under ambient conditions while very attractive, can be challenging. When a hydrogel is imaged in air (as was the case for STED imaging), it may be subject to water loss during imaging which can cause collapse of the structure and appear as channels in the images. An extreme example of such a collapsed structure is seen in the gel resulting from Critical Point Drying (CPD) (Fig. S2A, ESI†). However, when imaging a hydrogel immersed in a solution (as was the case for AFM imaging), its stability towards swelling/dehydration will depend on the chemistry of the polymer and the solution. For agarose gels of the current study, once the gel has set, it is not subject to swelling making it suitable for AFM imaging.[67] However, for gels made from other polymers such as ionic polymers, osmotic swelling will occur due to the charged groups on the polymer backbone. In this case, only gels that have attained their equilibrium water content can be imaged using AFM.

Common to STED and AFM is the requirement of choosing a threshold for where a pore wall ends and a pore starts. This introduces a bias in determination of the pore size distribution and highlights the importance to clearly describe this threshold in published work. A main advantage, therefore, of using Cryo-SEM in conjunction with careful freezing preparation is the 3D information of the gel and a clear distinction between the gel material and the vitreous ice.[1,11] Considering the relatively few studies using high pressure freezing prior to Cryo-SEM imaging, despite general acknowledgement of freezing artefacts as mentioned in the introduction, the main limitation of this technique is the highly specialised high pressure freezing preparation which is not commonly available and requires highly skilled staff for its correct execution.

Table 2 Advantages and limitations of direct visualisation methods used for pore size determination of hydrogels

Method	Advantages	Limitations
STED	• Hydrogel imaged in native state	• Polymer labelling required
	• Improved resolution compared to CLSM[17]	• Depending on the level of photobleaching of the fluorescent dye, capturing *z*-stack images may not be possible
	• Can image to different depths and regenerate 3D structure from *z*-stack	• Hydrated gel imaged at ambient humidity
	• Pore size determination can be done using automated approach[21,22,66]	• Threshold arbitrarily chosen
		• Still lower resolution than other techniques
AFM	• Hydrogel imaged in native state and using immersion chamber	• Limited to hydrogels of relative high polymer content due to the potential damage from the AFM tip[10,46]
	• High resolution	• Hydrogel must be stable when immersed in solution (*e.g.* does not undergo osmotic swelling)
	• Depth resolution quantifiable *via* in-built depth scale	• Imaging of hydrogel surface only
	• Pore size determination can be done using line plot approach	• Threshold arbitrarily chosen
Cryo-SEM	• High resolution (magnification 100 000×)	• High pressure freezing required for accurate pore size determination of high water-content hydrogels[1,11]
	• 3D information can be resolved	• Hydrogel imaged at low temperature and under vacuum
	• Pore wall and pore void easily discriminated	• Depth resolution not readily quantifiable
	• Can potentially image internal or external structure[1]	• Require manual approach for pore size determination

Based on the data collected in the current study, we found that images obtained using either STED, AFM or Cryo-SEM can be employed for the pore size determination of agarose gels with values in good agreement for gels with average pore sizes of 240 nm or smaller when using a manual approach for pore size determination. The fluorescence microscopy-based technique STED provided improved resolution compared to CLSM.[18,52,68] Deconvolution is an additional useful image post-processing step that improves resolution and signal-to-noise ratio of STED microscopy without the need to increase the beam intensity.[41] Manual approaches to pore size determination such as those used in the current study (line plot, manually inserting a circle) can be time-consuming and may introduce bias. Therefore, when the data permits, an automated approach could be used. The so-called ''bubble analysis'' method has previously been used for pore size determination of STED images based on the approaches outlined by Molteni *et al.* and Munster *et al.*[21,22,66]

5. Conclusion

Direct comparison of different techniques to image agarose gels has allowed us to evaluate their suitability in obtaining pore size distributions. For all images, the common manual approach to extracting pore size information was used. Validation of the use of this manual approach was achieved using PLGA nanoparticles as internal standard. Despite the different imaging environments and the distinctly different images that result from STED, AFM and Cryo-SEM, overall good agreement was found (pore sizes within 15%) for agarose gels of $>1.0\%$ which is equivalent to pore sizes of 240 nm and smaller. Gels of lower agarose concentrations are more prone to dehydration during imaging at ambient conditions while AFM is not suitable for gels of such low gel content. It is curious that AFM analysis resulted in a general lack of homogeneity across replicate gels for both concentrations evaluated, however, this may be a sample size effect and could be investigated further.

The main recommendations from this study are that (i) the use of CLSM for pore size analysis should be restricted to relatively large pore sizes, due to the resolution limits of the technique; (ii) when extracting pore size information from STED and AFM images, the threshold chosen to define where a pore wall end and the void start must be communicated to allow reproducibility, (iii) artefacts from the different techniques should be avoided, these include freezing artefacts for incorrect sample preparation for Cryo-SEM imaging, dehydration artefacts for low gel content gels imaged using STED, cantilever artefacts during imaging using AFM for gels of low gel content.

Conflicts of interest

There are no conflicts to declare.

Acknowledgements

The authors acknowledge helpful suggestions from Dr Gleb Yakubov. This work was performed in part at the Queensland node of the Australian National Fabrication Facility by Dr Elena Taran; a company established under the National Collaborative Research Infrastructure Strategy to provide nano and micro-fabrication facilities for Australia's researchers. The authors also acknowledge the facilities and the scientific and technical assistance of Dr Kim Sewell of the Australian Microscopy and Microanalysis Research Facility at the Centre of Microscopy and Microanalysis at The University of Queensland and Ms Tong Wu of the Queensland Branch of Olympus Australia. We acknowledge funding from the University of Queensland International Scholarship (IJ and BCG), ARC Centre of Excellence

in Bio-Nano Science (SRC) and ARC Laureate fellowship FL16010139 (AR).

References

1 R. Aston, K. Sewell, T. Klein, G. Lawrie and L. Grøndahl, Evaluation of the impact of freezing preparation techniques on the characterisation of alginate hydrogels by cryo-SEM, *Eur. Polym. J.*, 2016, **82**, 1–15.
2 N. R. Richbourg, A. Ravikumar and N. A. Peppas, Solute transport dependence on 3D geometry of hydrogel networks, *Macromol. Chem. Phys.*, 2021, **222**(16), 2100138.
3 Q. L. Loh and C. Choong, Three-dimensional scaffolds for tissue engineering applications: role of porosity and pore size, *Tissue Eng., Part B*, 2013, **19**(6), 485–502.
4 A. S. Hoffman, Hydrogels for biomedical applications, *Adv. Drug Delivery Rev.*, 2012, **64**, 18–23.
5 G. M. Cruise, D. S. Scharp and J. A. Hubbell, Characterization of permeability and network structure of interfacially photopolymerized poly (ethylene glycol) diacrylate hydrogels, *Biomaterials*, 1998, **19**(14), 1287–1294.
6 H.-W. Kang, Y. Tabata and Y. Ikada, Fabrication of porous gelatin scaffolds for tissue engineering, *Biomaterials*, 1999, **20**(14), 1339–1344.
7 A. Leal-Egaña, U.-D. Braumann, A. Díaz-Cuenca, M. Nowicki and A. Bader, Determination of pore size distribution at the cell-hydrogel interface, *J. Nanobiotechnol.*, 2011, **9**(1), 24.
8 N. Annabi, J. W. Nichol, X. Zhong, C. Ji, S. Koshy, A. Khademhosseini and F. Dehghani, Controlling the porosity and microarchitecture of hydrogels for tissue engineering, *Tissue Eng., Part B*, 2010, **16**(4), 371–383.
9 I. Jayawardena, K. Wilson, M. Plebanski, L. Grøndahl and S. Corrie, Morphology and Composition of Immunodiffusion Precipitin Complexes Evaluated via Microscopy and Proteomics, *J. Proteome Res.*, 2021, **20**(5), 2618–2627.
10 M. Oyen, Mechanical characterisation of hydrogel materials, *Int. Mater. Rev.*, 2014, **59**(1), 44–59.
11 Z. Kaberova, E. Karpushkin, M. Nevoralova, M. Vetrik, M. Slouf and M. Duskova-Smrckova, Microscopic Structure of Swollen Hydrogels by Scanning Electron and Light Microscopies: Artifacts and Reality, *Polymers*, 2020, **12**(3), 578.
12 H. J. Kong, E. Alsberg, D. Kaigler, K. Y. Lee and D. J. Mooney, Controlling degradation of hydrogels via the size of cross-linked junctions, *Adv. Mater.*, 2004, **16**(21), 1917–1921.
13 A. W. Chan and R. J. Neufeld, Modeling the controllable pH-responsive swelling and pore size of networked alginate based biomaterials, *Biomaterials*, 2009, **30**(30), 6119–6129.
14 H. Zhang and W. Davison, Diffusional characteristics of hydrogels used in DGT and DET techniques, *Anal. Chim. Acta*, 1999, **398**(2), 329–340.
15 J. J. Han, A. P. Shreve and J. H. Werner, Super-Resolution Optical Microscopy, *Characterization of Materials*, 2012, pp. 1–15.
16 U. V. Nägerl, K. I. Willig, B. Hein, S. W. Hell and T. Bonhoeffer, Live-cell imaging of dendritic spines by STED microscopy, *Proc. Natl. Acad. Sci. U. S. A.*, 2008, **105**(48), 18982–18987.
17 B. Huang, H. Babcock and X. Zhuang, Breaking the diffraction barrier: super-resolution imaging of cells, *Cell*, 2010, **143**(7), 1047–1058.
18 G. Dumbović, X. Sanjuan, M. Perucho and S.-V. Forcales, Stimulated emission depletion (STED) super resolution imaging of RNA-and protein-containing domains in fixed cells, *Methods*, 2021, **187**, 68–76.
19 L. G. Carvalhais, V. C. Martinho, E. Ferreiro and P. S. Pinheiro, Unraveling the nanoscopic organization and function of central mammalian presynapses with super-resolution microscopy, *Front. Neurosci.*, 2021, **14**, 578409.
20 S. W. Hell and J. Wichmann, Breaking the diffraction resolution limit by stimulated emission: stimulated-emission-depletion fluorescence microscopy, *Opt. Lett.*, 1994, **19**(11), 780–782.
21 M. Molteni, D. Magatti, B. Cardinali, M. Rocco and F. Ferri, Fast two-dimensional bubble analysis of biopolymer filamentous networks pore size from confocal microscopy thin data stacks, *Biophys. J.*, 2013, **104**(5), 1160–1169.
22 S. Münster and B. Fabry, A simplified implementation of the bubble analysis of biopolymer network pores, *Biophys. J.*, 2013, **104**(12), 2774.
23 J. Vandaele, B. Louis, K. Liu, R. Camacho, P. H. Kouwer and S. Rocha, Structural characterization of fibrous synthetic hydrogels using fluorescence microscopy, *Soft Matter*, 2020, **16**(17), 4210–4219.
24 N. L. Cuccia, S. Pothineni, B. Wu, J. Méndez Harper and J. C. Burton, Pore-size dependence and slow relaxation of hydrogel friction on smooth surfaces, *Proc. Natl. Acad. Sci. U. S. A.*, 2020, **117**(21), 11247–11256.
25 S. Shahab, M. Kasra and A. Dolatshahi-Pirouz, Design and construction of a novel measurement device for mechanical characterization of hydrogels: A case study, *PLoS One*, 2021, **16**(2), e0247727.
26 M. Caine, S. N. Bian, Y. Q. Tang, P. Garcia, A. Henman, M. Dreher, D. Daly, R. Carlisle, E. Stride, S. L. Willis and A. L. Lewis, In situ evaluation of spatiotemporal distribution of doxorubicin from Drug-eluting Beads in a tissue mimicking phantom, *Eur. J. Pharm. Sci.*, 2021, **160**, 105772.
27 M. Watase and K. Nishinari, Rheological properties of agarose gels with different molecular weights, *Rheol. Acta*, 1983, **22**(6), 580–587.
28 L. M. Barrangou, C. R. Daubert and E. A. Foegeding, Textural properties of agarose gels. I. Rheological and fracture properties, *Food Hydrocolloids*, 2006, **20**(2), 184–195.
29 V. Normand, D. L. Lootens, E. Amici, K. P. Plucknett and P. Aymard, New insight into agarose gel mechanical properties, *Biomacromolecules*, 2000, **1**(4), 730–738.
30 P. San Biagio, D. Bulone, A. Emanuele, M. Palma-Vittorelli and M. Palma, Spontaneous symmetry-breaking pathways: time-resolved study of agarose gelation, *Food Hydrocolloids*, 1996, **10**(1), 91–97.
31 K. Bertula, L. Martikainen, P. Munne, S. Hietala, J. Klefström and O. Ikkala, Nonappa, Strain-stiffening of agarose gels, *ACS Macro Lett.*, 2019, **8**(6), 670–675.

32 M. Martinez-Sanz, A. Strom, P. Lopez-Sanchez, S. H. Knutsen, S. Ballance, H. K. Zobel, A. Sokolova, E. P. Gilbert and A. Lopez-Rubio, Advanced structural characterisation of agar-based hydrogels: Rheological and small angle scattering studies, *Carbohydr. Polym.*, 2020, **236**, 115655.

33 J. Peng, Q. Pan, W. Zhang, H. Yang, X. Zhou and H. Jiang, Effects of DS-modified agarose gels on neurite extension in 3D scaffold through mechanisms other than changing the pore radius of the gels, *J. Biomed. Mater. Res., Part A*, 2014, **102**(7), 2157–2162.

34 H. Hezaveh, S. Cosson, E. A. Otte, G. Su, B. D. Fairbanks and J. J. Cooper-White, Encoding stem-cell-secreted extracellular matrix protein capture in two and three dimensions using protein binding peptides, *Biomacromolecules*, 2018, **19**(3), 721–730.

35 J. Liang, F. Teng, T.-M. Chou and M. Libera, Measuring microgel swell ratio by cryo-SEM, *Polymer*, 2017, **116**, 1–4.

36 L. Yu, G. E. Yakubov, E. P. Gilbert, K. Sewell, A. M. van de Meene and J. R. Stokes, Multi-scale assembly of hydrogels formed by highly branched arabinoxylans from Plantago ovata seed mucilage studied by USANS/SANS and rheology, *Carbohydr. Polym.*, 2019, **207**, 333–342.

37 N. Russ, B. I. Zielbauer, K. Koynov and T. A. Vilgis, Influence of nongelling hydrocolloids on the gelation of agarose, *Biomacromolecules*, 2013, **14**(11), 4116–4124.

38 N. Ioannidis, J. Bowen, A. Pacek and Z. Zhang, Manufacturing of agarose-based chromatographic adsorbents–effect of ionic strength and cooling conditions on particle structure and mechanical strength, *J. Colloid Interface Sci.*, 2012, **367**(1), 153–160.

39 C. Chen, X. Li, D. Zhao, Y. Li, H. Shi, G. Ma and Z. Su, Precise control of agarose media pore structure by regulating cooling rate, *J. Sep. Sci.*, 2017, **40**(22), 4467–4474.

40 B. C. Garms, H. Poli, D. Baggley, F. Y. Han, A. K. Whittaker, A. Anitha and L. Grøndahl, Evaluating the effect of synthesis, isolation, and characterisation variables on reported particle size and dispersity of drug loaded PLGA nanoparticles, *Mater. Adv.*, 2021, **2**(17), 5657–5671.

41 G. Vicidomini, P. Bianchini and A. Diaspro, STED super-resolved microscopy, *Nat. Methods*, 2018, **15**(3), 173.

42 E. Ukraintsev, A. Kromka, H. Kozak, Z. Remeš and B. Rezek, Artifacts in atomic force microscopy of biological samples, in *Atomic Force Microscopy Investigations into Biology-From Cell to Protein*, ed. C. L. Frewin, InTech, 2012, pp. 29–54.

43 K. Wadu-Mesthrige, N. A. Amro, J. C. Garno, S. Cruchon-Dupeyrat and G.-Y. Liu, Contact resonance imaging—a simple approach to improve the resolution of AFM for biological and polymeric materials, *Appl. Surf. Sci.*, 2001, **175**, 391–398.

44 N. Pernodet, M. Maaloum and B. Tinland, Pore size of agarose gels by atomic force microscopy, *Electrophoresis*, 1997, **18**(1), 55–58.

45 K. Westra, A. Mitchell and D. Thomson, Tip artifacts in atomic force microscope imaging of thin film surfaces, *J. Appl. Phys.*, 1993, **74**(5), 3608–3610.

46 M. Maaloum, N. Pernodet and B. Tinland, Agarose gel structure using atomic force microscopy: gel concentration and ionic strength effects, *Electrophoresis*, 1998, **19**(10), 1606–1610.

47 L.-B. Cao, S. Zeng and W. Zhao, Highly stable PEGylated poly (lactic-*co*-glycolic acid)(PLGA) nanoparticles for the effective delivery of docetaxel in prostate cancers, *Nanoscale Res. Lett.*, 2016, **11**(1), 1–9.

48 A. A. Shitole, N. Sharma, P. Giram, A. Khandwekar, M. Baruah, B. Garnaik and S. Koratkar, LHRH-conjugated, PEGylated, poly-lactide-*co*-glycolide nanocapsules for targeted delivery of combinational chemotherapeutic drugs Docetaxel and Quercetin for prostate cancer, *Mater. Sci. Eng., C*, 2020, **114**, 111035.

49 V. Kestens, T. Gerganova, G. Roebben and A. Held, A new certified reference material for size and shape analysis of nanorods using electron microscopy, *Anal. Bioanal. Chem.*, 2021, **413**(1), 141–157.

50 M. M. Chui, R. J. Phillips and M. J. McCarthy, Measurement of the porous microstructure of hydrogels by nuclear magnetic resonance, *J. Colloid Interface Sci.*, 1995, **174**(2), 336–344.

51 C. S. Hansel, M. N. Holme, S. Gopal and M. M. Stevens, Advances in high-resolution microscopy for the study of intracellular interactions with biomaterials, *Biomaterials*, 2020, **226**, 119406.

52 L. G. Carvalhais, V. C. Martinho, E. Ferreiro and P. S. Pinheiro, Unraveling the Nanoscopic Organization and Function of Central Mammalian Presynapses With Super-Resolution Microscopy, *Front Neurosci-Switz*, 2021, **14**, 578409.

53 J. Narayanan, J. Y. Xiong and X. Y. Liu, Determination of agarose gel pore size: Absorbance measurements vis a vis other techniques, *J. Phys. Conf. Ser.*, 2006, **28**(1), 83–86.

54 B. Tinland, N. Pernodet and G. Weill, Field and pore size dependence of the electrophoretic mobility of DNA: a combination of fluorescence recovery after photobleaching and electric birefringence measurements, *Electrophoresis*, 1996, **17**(6), 1046–1051.

55 C. Huang, H. Kobayashi, M. Moritaka and M. Okubo, Hollow particles are produced by the burying of sulfate end-groups inside particles prepared by emulsion polymerization of styrene with potassium persulfate as initiator in the absence/presence of a nonionic emulsifier, *Polym. Chem.*, 2017, **8**(45), 6972–6980.

56 N. H. Olson and T. S. Baker, Magnification calibration and the determination of spherical virus diameters using cryo-microscopy, *Ultramicroscopy*, 1989, **30**(3), 281–298.

57 M. Cermola and W. H. Schreil, Size changes of polystyrene latex particles in the electron microscope under controlled physical conditions, *J. Electron Microsc. Tech.*, 1987, **5**(2), 171–179.

58 D. Karamata, Polystyrene spheres in electron microscopy, *J. Ultrastruct. Res.*, 1971, **35**(3), 201–209.

59 S. D. Duke and E. B. Layendecker, In Internal standard method for size calibration of sub-micrometer spherical particles by electron microscope, Technical Note presented at Fine Particle Society Meeting. June, 2003.

60 J. H. Watson and W. L. Grube, The reliability of internal standards for calibrating electron microscopes, *J. Appl. Phys.*, 1952, **23**(7), 793–798.
61 P. C. Braga and D. Ricci, *Atomic force microscopy: biomedical methods and applications*, Springer Science & Business Media, 2004, vol. 242.
62 P. Aymard, D. R. Martin, K. Plucknett, T. J. Foster, A. H. Clark and I. T. Norton, Influence of thermal history on the structural and mechanical properties of agarose gels, *Biopolymers*, 2001, **59**(3), 131–144.
63 L. Jiang and S. Granick, Real-space, in situ maps of hydrogel pores, *ACS Nano*, 2016, **11**(1), 204–212.
64 L. Kisley, R. Brunetti, L. J. Tauzin, B. Shuang, X. Yi, A. W. Kirkeminde, D. A. Higgins, S. Weiss and C. F. Landes, Characterization of porous materials by fluorescence correlation spectroscopy super-resolution optical fluctuation imaging, *ACS Nano*, 2015, **9**(9), 9158–9166.
65 J. Rahbani, A. R. Behzad, N. M. Khashab and M. Al-Ghoul, Characterization of internal structure of hydrated agar and gelatin matrices by cryo-SEM, *Electrophoresis*, 2013, **34**(3), 405–408.
66 M. Molteni, D. Magatti, B. Cardinali, M. Rocco and F. Ferri, Response to ''a simplified implementation of the bubble analysis of biopolymer networks pores'', *Biophys. J.*, 2013, **104**(12), 2776–2777.
67 A. Hayashi and T. Kanzaki, Swelling of agarose gel and its related changes, *Food Hydrocolloids*, 1987, **1**(4), 317–325.
68 Z. Y. Wu, X. Z. Xu and P. Xi, Stimulated emission depletion microscopy for biological imaging in four dimensions: A review, *Microsc. Res. Tech.*, 2021, 1947–1958.